Aerosol and Air Quality Research, 16: 1793–1804, 2016

ISSN: 1680-8584 print / 2071-1409 online
doi: 10.4209/aaqr.2015.04.0205

Characterization of Background Aerosol Properties during a Wintertime Smog Episode

Agnes Molnár[1], Zsuzsanna Bécsi[2], Kornélia Imre[1*], Vera Gácser[2], Zita Ferenczi[3]

[1] *MTA-PE Air Chemistry Research Group, Veszprém, P.O. Box 158, H-8201, Hungary*
[2] *University of Pannonia, Veszprém, P.O. Box 158, H-8201, Hungary*
[3] *Hungarian Meteorological Service, Budapest P.O. Box 39, H-1186 Hungary*

ABSTRACT

The aim of this paper is to study the wintertime physical properties of atmospheric aerosol particles on the basis of data observed at the K-puszta regional background station in Hungary. In Hungary wintertime smog episodes are linked to strong stable air (high pressure blocking events) with thermal inversion. These atmospheric conditions are frequently formed during winter months (November–February) due to the special geographical location of the country. The formation of smog events is highly probable in cases of thermal inversion periods sustaining for at least 4 days. We discuss in the paper the role of high-pressure blocking events in aerosol properties in terms of PM_{10} concentrations, aerosol size distributions, new particle formation and optical properties. We found that high-pressure blocking events have significant impacts on the size distribution and particle formation processes. At K-puszta the aerosol is in highly aged state with size distribution dominated by the accumulation mode. This is further supported by the optical properties, e.g., by high scattering Ångstrom exponent and by relatively weak absorption. The most significant effect of extreme episodes is manifested in the changes in PM_{10} concentrations and, consequently, in aerosol optical properties. The PM_{10} concentrations, scattering coefficients and absorption coefficients considerably increase to extreme values that are characteristic of a heavily polluted atmosphere rather than rural air. Our results indicate that in winter, the air quality at K-puszta is often influenced by regional air pollution as shown by spatial distribution of PM_{10} concentration. It is found that PM_{10} had almost the same concentration in regional background air and in different types of urban environments. The special meteorological conditions and the role of regional-scale transport can explain why local abatements in cities cannot lead to significant improvement of the air quality during smog events.

Keywords: PM_{10}; Aerosol size distribution; Particle formation; Scattering and absorption; Air pollution episode.

INTRODUCTION

Important air pollution episodes regularly occur during the winter months. Deterioration of air quality is receiving attention in urban environments because it plays an important role in our everyday life, from public health issues to the economy. Elevated levels of air pollutants directly and indirectly affect human health, aerosol optical properties and visual range. The health impacts of air pollution are mainly associated with respiratory and cardiovascular diseases, which lead to higher mortality and morbidity in particularly vulnerable populations.

It is well established that air quality and weather events are interrelated: meteorological situations frequently lead to negative impacts on urban and rural air quality (see London Great Smog in 1952 or photochemical smog in large cities, such as Los Angeles). From the first appearance of great London smog until recent days, wintertime smog is a well-known phenomenon affecting urban, background and remote environments all over the world. (e.g., Ram *et al.*, 2012; Zotter *et al.*, 2013; Guo *et al.*, 2014; Jiang *et al.*, 2015).

Air quality depends on a number of factors, most notably, the sources of primary air pollutants. In addition, meteorology can also significantly contribute to the formation of smog episodes, which can be further aggravated by unfavorable topography (i.e., mountainous areas and basins). Severe urban air pollution episodes can form in winter and persist for several days to weeks. Smog events are closely related to atmospheric stability and generally form during cold temperatures and weak winds (e.g., Guo *et al.*, 2014; Jiang *et al.*, 2015; Yuan *et al.*, 2015; Zheng *et al.*, 2015). Under strong stable air, horizontal and vertical mixing are limited due to the development of a thermal inversion layer;

* Corresponding author.
Tel.: +36-88-624-000/6054
E-mail address: kornelia@almos.uni-pannon.hu

consequently, the concentration of atmospheric constituents can be extremely high.

In Hungary the formation of strong stable atmospheric conditions is strongly affected by the geographical location of the country. Hungary can be found in a basin surrounded by the Carpathians, the Alps and the Dinaric Alps. Generally due to a cold front the total space of the Carpathian basin is filled with cold air. After the passage of the cold front an anticyclone builds up with lessening winds and calm weather. At night the surface strongly cools down as a consequence of clear sky and intensive surface radiation (especially in case of snow cover); and a quickly growing radiation inversion is formed above the surface that generally extends to the whole Carpathian basin with an average height of 300–600 m (Cséki, 2010).

These atmospheric conditions frequently formed during winter months. According to a comprehensive study (1988–2008) the number of wintertime thermal inversion over Hungary sustaining for 4 or more days is rather high, they occur 6 times per year on the average (Cséki, 2010). It has to be mentioned that the formation of smog episodes are linked to these longer periods. In the last years (2007–2012) the wintertime inversion periods still occurred regularly which is shown in Table. 1. Each wintertime during the 6 years inversion periods have been formed about 4–7 times, the longest period lasted 33 days. During these periods the PM_{10} well describes the scale of air quality.

The wintertime pollution episodes are normally linked to a number of air pollutants like aerosol mass concentration (PM) and trace gases. Over the past few decades, the emission and concentration of SO_2 have decreased significantly in most European countries; however, bad air quality due to the occurrence of winter-type smog episodes is still a serious problem in several European cities (Richter and Peter Williams, 1998). For example, episodes of high ambient PM_{10} concentrations (exceeding the EU limit value of 50 $\mu g\ m^{-3}$) occur regularly in Ostrava (Czech Republic) (Baranova and Hovorka, 2013), Krakow (Poland) (Larsen *et al.*, 2008) and Budapest, Hungary in winter as indicated by smog alerts of the recent years. This means that due to the emission mitigation policy, among the air pollutants PM plays a major role in these episodes. In Hungary under wintertime smog events the concentrations of SO_2 and NO_2 increase similarly to other observations obtained e.g., in China, Asia (Jiang *et al.*, 2015), however, unlike PM_{10}, their concentration only rarely exceeds the 24-hours health standards. Recently, winter smog episodes have been mainly characterized by the high exposure of particulate matter. Fine fraction of PM obviously plays a very important role in haze and smog formation. The contribution of secondary species (e.g., organic compounds, sulfate, nitrate, and ammonium) in fine PM is generally high suggesting the significance of secondary aerosol formation most likely via heterogeneous reactions (Jiang *et al.*, 2015; Zheng *et al.*, 2015). The mass concentration of aerosol particles, mainly in the fine fraction is influenced by long-range transport (Richter and Peter Williams, 1998; Ferenczi, 2013). According to EEA (2013), in several European countries significant fractions of $PM_{2.5}$ (sometimes > 50%) can be attributed to long-range transport. As a result, air pollution episodes cannot be confined exclusively to urban air; they also affect the background or rural air quality. Smog areas can even extend to 100–1000 km^2 (Breiling, 1993).

One of the best known manifestations of the long-range transport of anthropogenic air pollutants is Arctic haze. Arctic haze is mainly a result of increased anthropogenic aerosol loads from northern Europe and northern Russia. During winter and early spring, a high concentration of accumulation mode particles can be measured in the Arctic. The episode may last from a few days to weeks when strong surface-based temperature inversion forms, which is characterized by a cold, stable atmosphere that inhibits vertical mixing and the formation of cloud systems and precipitation (Quinn *et al.*, 2007).

The main focus of this work is to study the different aerosol parameters under a typical wintertime smog episode in Carpathian basin. Between 2007 and 2012 there were several sustained smog periods when the air pollution built up; and at the beginning of 2010 a quite long period occurred which was highly appropriate for a general characterization of wintertime smog periods. The changes in aerosol number and PM_{10} concentrations, the aerosol size distribution and the aerosol optical properties are discussed as a function of the meteorological conditions.

INSTRUMENTATION AND METHODS

Site Description

All of the measurements were conducted at the K-puszta station in 2010. The K-puszta background air pollution monitoring station is a rural measurement site located in Hungary (46°58'N, 19°35'E, 125 m a.s.l.) on the Great Hungarian Plain, 15 km northwest of the nearest town of Kecskemét and 70 km southeast of Budapest. The station belongs to the Global Atmosphere Watch (GAW) and European Monitoring and Evaluation Programme (EMEP)

Table 1. Smog period statistic between 2007 and 2012 at K-puszta and Budapest.

Winter	Number of smog period	Duration of smog period [days] (min–max)	PM_{10} concentration [$\mu g\ m^{-3}$]			
			Non-smog period		Smog period	
			Budapest	K-puszta	Budapest	K-puszta
2007/2008	7	60 (4–33)	33.0	25.1	54.4	48.6
2008/2009	4	36 (3–23)	25.4	23.5	55.1	59.1
2009/2010	5	62 (5–29)	27.5	28.4	46.7	52.9
2010/2011	6	51 (6–11)	28.3	n.a	54.4	n.a
2011/2012	6	44 (4–20)	19.5	18.4	50.6	35.0

networks, and it is one of the EUSAAR supersites. The surroundings of the station are dominated by mixed forest (62% coniferous and 28% deciduous) and grassland (10%), and the soil around the site is sandy.

For comparison, we used PM_{10} and meteorological data measured at Budapest, (Marczell György Observatory, Hungarian Meteorological Service) which is a suburban sampling site in a residential area (47.42°N; 19.18°E), affected by local pollution mainly from traffic and residential heating.

DMPS Measurements

The aerosol number size distribution is monitored by a DMPS (Differential Mobility Particle Sizer) (Aalto *et al.*, 2001); the size distributions of aerosol particles in the 5–800 nm size range are measured approximately every 10 minutes. The particles are classified according to their electrical mobility; then the number concentration of the particles in different size classes is measured by a condensation particle counter (TSI3772).

The aerosols are sampled at a height of two meters and one meter from the station wall. No special inlet is used (only a rain cover). The sampling line is 4 mm diameter copper tubing. Ni-63 370 MBq aerosol neutralizer is applied, and the aerosol classifier is a copy of a Hauke-type 28 cm long DMA. The aerosols are dried with a Topas aerosol drier. Because a drier is used, the size distribution of dry particles is measured.

Aerosol Optics

The optical properties of aerosol particles < 10 μm are discussed. The NOAA-type sampling inlet is 10 m above the surface. The sampled air is dried prior to entering the instruments using a Permapure heatless dryer by diluting the dry particle-free air; the relative humidity of the sampled air is kept under 50%.

The scattering and backscattering coefficients are measured by an integrating nephelometer (TSI3565) at wavelengths of 450, 550 and 700 nm. The averaging time and the sampling rate are 1 min and 29.5 L min^{-1}, respectively. The nephelometer measures the light intensity scattered between 7° and 170°. The scattering coefficients are corrected for truncation error according to Anderson and Ogren (1998). Regarding the 1 min averaging time, the detection limits of the scattering coefficients at 450, 550 and 700 nm are 0.65, 0.25 and 0.38 Mm^{-1}, respectively (Anderson *et al.*, 1996). A span gas check (filtered air (low span) and CO_2 (high span)) is conducted monthly, and zero background check is performed every hour.

The aerosol light absorption is measured by a Particle Soot Absorption Photometer (PSAP). This instrument works at 565 nm wavelength, which is extrapolated to 550 nm using the Ångström exponent (α) of –1 (Müller *et al.*, 2011). In the PSAP, a filter-based method is used to measure the absorption coefficient (Bond *et al.*, 1999). The transmittance and the derived absorption coefficient depend on the particle load of the filter, the light scattering of the particles deposited on the filter, the flow rate and the spot size. The absorption coefficients are corrected for these parameters (Bond *et al.*, 1999). When the filter transmittance reaches 70%, the filter is changed; in cases where the transmittance is below 70%, the absorption coefficients are disregarded. In the case of the PSAP, the flow rate and the averaging time is 0.3 L min^{-1} and 1 min, respectively. This instrument was involved in an intercomparison of aerosol absorption photometers in 2005 and 2007 (Müller *et al.*, 2011).

PM_{10} and Meteorology

A standard automatic meteorological station, which is operated by the Hungarian Meteorological Service, is installed at the sampling site. The surface (i.e., 2 m height) temperature, relative humidity, air pressure, global radiation, precipitation and wind speed are measured in 10-minute intervals. Similarly, PM_{10} concentrations are also available with a 30-minute time resolution. At both sampling sites PM_{10} were measured by a beta-gauge particulate monitor. Finally, the height of the planetary boundary layer is calculated every 3 hours by the ECMWF (The European Centre for Medium-Range Weather Forecasts).

METHODS

Classifying Particle Formation Events

Particle formation events are classified on the basis of daily (00:00–24:00) DMPS spectra according to the classification scheme recommended by Yli-Juuti *et al.* (2009). The classification is performed visually by a three-person group to minimize the subjectivity. The days are classified into events, non-events, or undefined data groups. On event days, particle formations are intense and a distinctly new particle mode (i.e., nucleation mode; < 25 nm) is observed (Dal Maso *et al.*, 2005). Non-event days are generally characterized by a bimodal size distribution in which particles < 25 nm are lacking. On undefined days, particles < 25 nm are often present but without a distinct new particle mode. The summary of the event classification for the study period is presented in Table 2.

Size Distribution

The aerosol size distribution is discussed in terms of the modal particle size of nucleation, Aitken and accumulation size ranges. The modal particle diameters are calculated as (Eq. (1)):

$$ND = \frac{\sum_{5}^{25} d_i \cdot C_i}{\sum_{5}^{25} C_i},\ AiD = \frac{\sum_{25}^{100} d_i \cdot C_i}{\sum_{25}^{100} C_i},$$
$$AcD = \frac{\sum_{100}^{800} d_i \cdot C_i}{\sum_{100}^{800} C_i},\ TD = \frac{\sum_{5}^{800} d_i \cdot C_i}{\sum_{5}^{800} C_i} \quad (1)$$

where *N*, *Ai* and *Ac* denote the nucleation, Aitken and accumulation modes, respectively. The cut-off diameters of 25 and 100 nm are applied according to the recommendation of Dal Maso *et al.* (2005). The total mean particle size (TD) is calculated as above but over the entire 5–800 nm size

Table 2. NPF event classification statistics in January–February, 2010.

Event class	Days		
	Total data	Smog episode	Non-smog period
Events	6	2	4
Non-events	39	28	11
Undefined	6	4	2
Total classified days	51	34	17

range. The number concentration fractions in the nucleation, Aitken and accumulation size ranges are computed as follows (Eq. (2)):

$$N\% = \frac{\sum_{5}^{25} C_i}{\sum_{5}^{800} C_i} \cdot 100,\ Ai\% = \frac{\sum_{25}^{100} C_i}{\sum_{5}^{800} C_i} \cdot 100,$$
$$Ac\% = \frac{\sum_{100}^{800} C_i}{\sum_{5}^{800} C_i} \cdot 100 \quad (2)$$

Derived Intensive Optical Properties: Single Scattering Albedo, Ångström Exponent, and Hemispheric Backscattering Ratio

Additionally, intensive optical properties, such as single-scattering albedo (at 550 nm), the backscattering fractions (at wavelengths of 450, 550 and 700 nm), and the Ångström exponents for the total and backscattering coefficients are discussed. The single scattering albedo (ω_0) is defined as the ratio of the scattering and the extinction (scattering + absorption) coefficients. The backscattering coefficient ($\sigma_{bsc,\lambda}$) measured by the nephelometer is the scattered light intensity in the backward hemisphere of the particle (90°–180°). The hemispheric backscatter (b_λ) fraction is the ratio of the backscattering coefficient and the total scattering (e.g., Seinfeld and Pandis, 1998).

The scattering Ångström exponent is an efficient way to study the aerosol size distribution and obtain information on air pollution as first proposed by Junge (1963) because it is inversely related to particle size. For aerosols dominated by submicrometer particles, the scattering Ångström exponent is large, while for coarse particles, the value is low (e.g., Pereira *et al.*, 2011). The scattering Ångström exponent is calculated as (Eq. (3)):

$$\alpha_{sc}\left(\frac{\lambda_1}{\lambda_2}\right) = -\frac{\log\left(\frac{\alpha_{sc,\lambda_1}}{\alpha_{sc,\lambda_2}}\right)}{\log\left(\frac{\lambda_1}{\lambda_2}\right)} \quad (3)$$

Meteorology

By 13th of January of 2010 an anticyclone extended over the Carpathian Basin and the impact of high pressure weather system was dominant in the next weeks. The thermal structure of the atmosphere was studied by using the radiosonde records carried out in Budapest (Budapest, UWYO, 2014). The inversion evolved in one day – over the 900 hPa level – and parallel to this PM_{10} concentration increased day by day. The height of the inversion layer changed according to the variation of the weather situation, but the regular attendance of the inversion was found in the lower troposphere till the middle of February. Because of the lack of intensive fronts, a persistent air pollution episode occurred, which greatly affected the air quality over K-puszta. During the smog event the ambient temperature significantly decreased, along with weak easterly surface winds (see Table 3). Owing to cold air pool the mixing layer depth was very low (240 m on average) which favors the development of extreme air pollution. In Fig. 1 the European weather situation is shown at the beginning of the smog period and on January 28, 2010 when the highest PM_{10} was measured at K-puszta. One can see on both maps that an anticyclone over the East-European Plain and Central-Europe played decisive role in the control of the weather in Hungary.

RESULTS AND DISCUSSION

PM_{10}, Number Concentration and Number Size Distribution

During the entire study period (January–February, 2010), the daily average PM_{10} concentration was rather high (Table 4) and reached the 24-hour threshold limit (50 μgm^{-3}). During the smog, the daily average PM_{10} (60.5 μgm^{-3}) was nearly twice as high as the concentration prior to and after the episode (32.0 $\mu g\ m^{-3}$) (Table 4). As shown in Fig. 2, in several cases, the aerosol mass concentration briefly exceeded 100 $\mu g\ m^{-3}$. Such high PM_{10} concentrations generally characterize plumes of biomass burning or other smoky air masses (Garland *et al.*, 2008). In some cases, the PM_{10} shows low concentration, probably due to favorable weather conditions (e.g., higher wind speed).

The average aerosol number concentration (TC) was 7115 particles cm^{-3} (in the 5–800 nm size range). Although the average number concentration was higher in the smog (7355 cm^{-3}) than in the non-smog period (6501 cm^{-3}), this higher number concentration could be attributed to the inhibited vertical mixing and weak aerosol removal processes (cloud and precipitation removal), as seen with Arctic haze episodes (Quinn *et al.*, 2007). Generally, in Hungary, winter is the least active period in terms of new particle formation (NPF) processes (Bécsi *et al.*, 2013) due to unfavorable atmospheric conditions and the low biological activity of the surrounding vegetation. The lowest NPF rate was found during the smog episode (0.054 event/day), while beyond this period the formation rate was three times higher (0.182 event/day). The inactivity of nucleation processes is

further supported by the low percentage of nucleation mode aerosols (N% = 5%, see Table 4). The wintertime aerosols at K-puszta were rather aged, as shown by the relationship between the accumulation mode number concentration and PM_{10} (Table 5), i.e., PM_{10} is generally controlled by the accumulation mode particles.

Table 3. Summary of averaged meteorological parameters.

	Temperature (°C)	Wind speed (m s^{-1})	Pressure (hPa)	Average precipitation (mm)	Relative humidity (%)
January–February, 2010	–0.8 ± 4.9	1.9 ± 1.1	997.0 ± 10.5	2.6	88.4 ± 10.0
Smog episode	–2.5 ± 4.1	1.7 ± 1.0	1001.3 ± 9.7	0.7	87.9 ± 9.2
Non-smog period	2.1 ± 4.8	2.2 ± 1.3	989.7 ± 7.3	5.7	89.1 ± 11.2

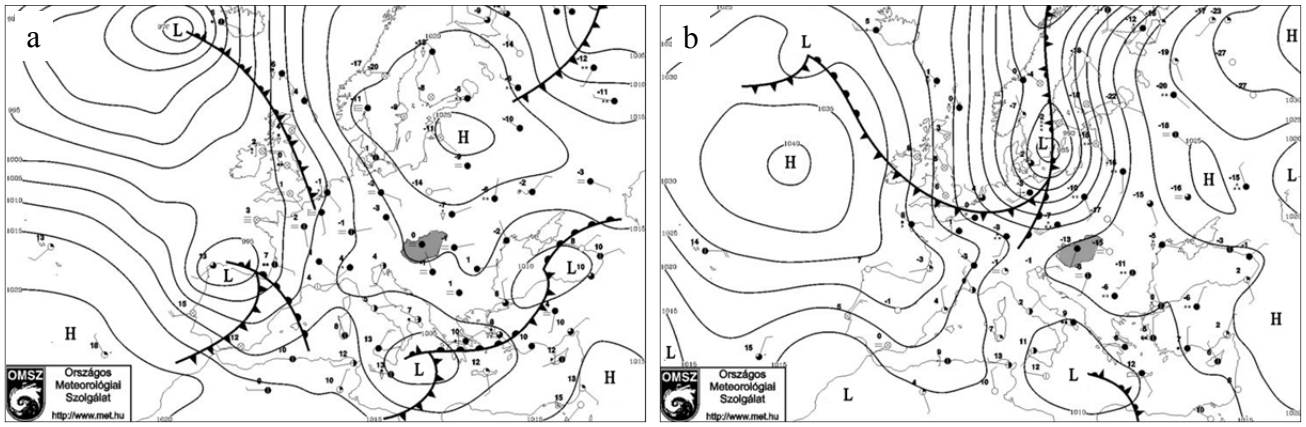

Fig. 1. European weather situation (a) at the beginning of the smog period (January 14, 2010. 00 UTC) and (b) on January 28, 2010 when the highest PM_{10} was measured at K-puszta (H: high pressure, L: low pressure).

Table 4. Summary of aerosol characteristics during the entire studied period (January–February, 2010), the smog episode and beyond.

		All days	Smog episode	Non-smog
PM_{10} (μg m^{-3})		49.9 ± 26.2	60.5 ± 24.5	32.0 ± 18.0
New particle formation	Event number	6	2	4
	NPF episode/day	0.118	0.054	0.182
Number concentration (cm^{-3})	Total	7115 ± 3155	7355 ± 3014	6501 ± 3419
	Nucleation	443 ± 720	390 ± 624	578 ± 909
	Aitken	3163 ± 2006	3114 ± 1863	3286 ± 2330
	Accumulation	3507 ± 1593	3846 ± 1586	2637 ± 1243
Modal diameter (nm)	Total	127 ± 23	133 ± 19	112 ± 25
	Nucleation	19 ± 2	20 ± 2	19 ± 2
	Aitken	65 ± 6	66 ± 5	62 ± 7
	Accumulation	193 ± 11	196 ± 9	184 ± 12
Modal fraction (%)	Nucleation	6 ± 6	5 ± 4	8 ± 9
	Aitken	43 ± 10	41 ± 9	48 ± 12
	Accumulation	51 ± 13	53 ± 11	44 ± 15
Total scattering (Mm^{-1})	450 nm	246.8 ± 141.9	301.7 ± 137.1	159.4 ± 99.3
	550 nm	175.2 ± 103.7	215.6 ± 100.2	110.9 ± 71.8
	700 nm	108.2 ± 66.3	134.1 ± 64.4	67.2 ± 45.1
Absorption (Mm^{-1})	550 nm	14.1 ± 7.8	16.7 ± 7.9	11.0 ± 6.6
Extinction coefficient (Mm^{-1})	550 nm	164.2 ± 90.8	203.8 ± 81.3	117.1 ± 78.2
Single scattering albedo	550 nm	90.8 ± 2.8	91.7 ± 2.1	89.7 ± 3.2
Hemispheric backscatter fraction (%)	450 nm	10.2 ± 1.0	9.9 ± 0.8	10.7 ± 1.2
	550 nm	11.4 ± 1.5	11.0 ± 1.1	12.1 ± 1.6
	700 nm	15.4 ± 2.0	14.7 ± 1.6	16.3 ± 2.2
Ångström exponent (total scattering)	450/700	1.92 ± 0.21	1.86 ± 0.20	2.01 ± 0.18
Ångström exponent (back-scattering)	450/700	1.01 ± 0.12	0.98 ± 0.11	1.06 ± 0.11

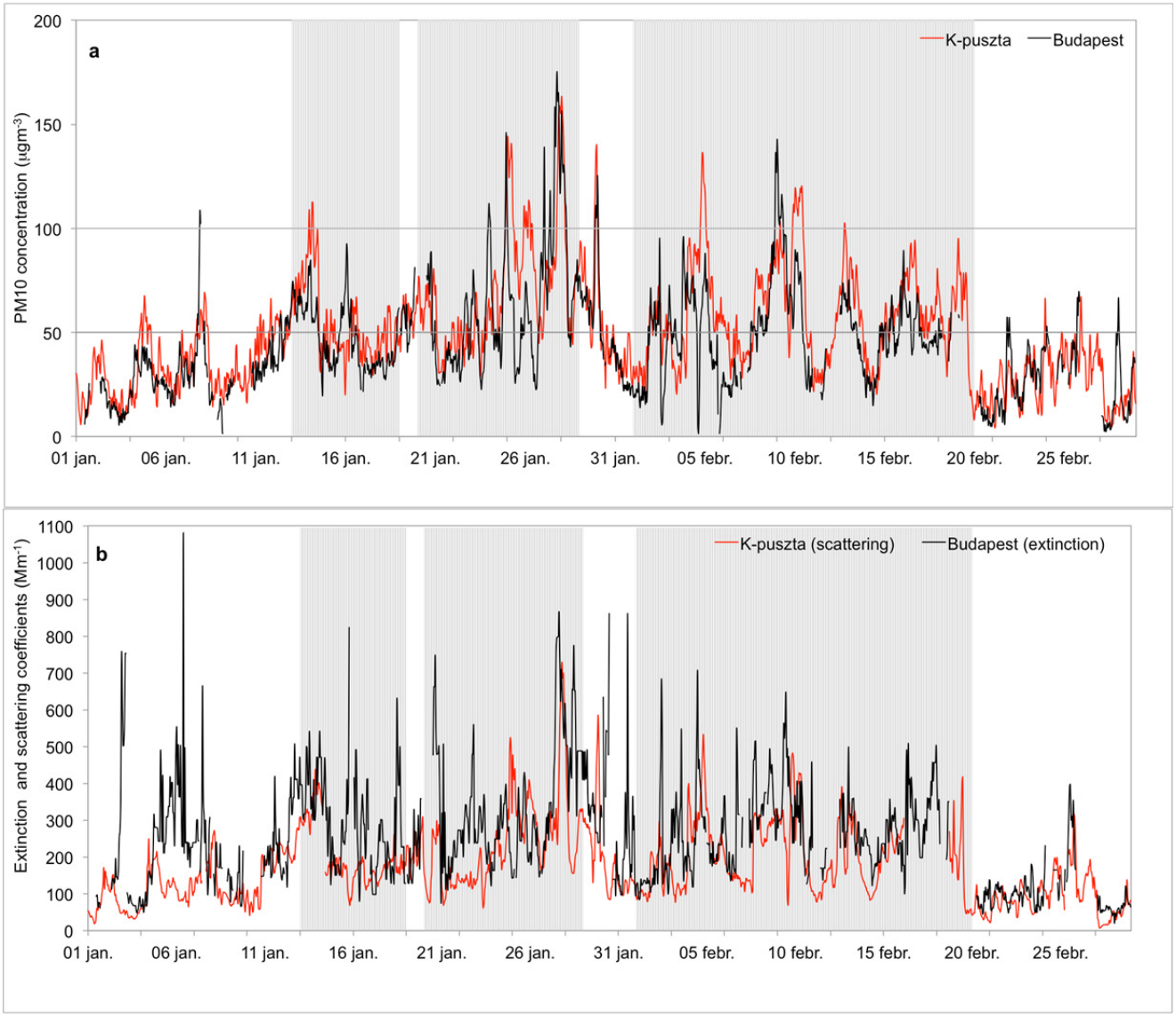

Fig. 2. PM_{10} concentration (a) and scattering/extinction coefficients (b) at K-puszta and Budapest, January–February, 2010 (gray periods: inversion periods).

As shown in Figs. 3 (a) and 3(b), the average number size distributions in the smog and non-smog periods were multimodal, with modes in the Aitken and accumulation size ranges. Under smog, the number concentration was dominated by the accumulation mode (Ac% = 53%) with a 41% contribution of the Aitken mode. The deconvolution of the number size distribution showed a relatively small peak in the Aitken mode at 53 nm. Significant modes were found at 103 nm and 165 nm. The former presumably contained particles both from the Aitken and the accumulation size ranges as the results of coagulation and condensation processes. Beside the peak at 165 nm a non-negligible mode was also found at 278 nm. These all resulted in a total mean diameter (TD) of 133 nm. The number size distribution suggests an aged aerosol at K-puszta, contrary to the results obtained in Reno, Nevada, where the elevated PM_{10} corresponded to freshly emitted aerosols (Gyawali *et al.*, 2012). Larsen *et al.* (2008) also concluded that in the region of Krakow (Poland), the combination of coal combustion, traffic exhaust and the atmospheric conditions (low winds, temperature inversion) could be blamed for similar pollution events. Contrary, Baranova and Hovorka (2013) found that in Ostrava, Czech Republic the average number size distribution during smog episodes was nearly monomodal with a mode at 150 nm.

Beyond the smog, the TD decreased by 21 nm (see Table 4) as a consequence of the modified shares of the Aitken and accumulation modes (48% and 44%, respectively). The number size distribution (Fig. 3(b)) was characterized by a mode at 62 nm in the Aitken size range, and three other peaks in the accumulation mode (at 130 nm, 225 nm and 382 nm). In Ostrava, Baranova and Hovorka (2013) also observed a bimodal size distribution after the pollution episode; however their results substantially differed from the size distribution obtained at K-puszta. They found a first mode at 25 nm and a second at 55 nm. The mode at 25 nm indicates

Table 5. Statistical relationship of PM_{10}, total and modal number concentrations, diameters and modal fractions with aerosol optical characteristics and meteorological parameters[a].

	PM_{10}	Number concentration (cm^{-3})				Modal diameter (nm)				Modal fractions (%)		
		T	N	Ai	Ac	T	N	Ai	Ac	N%	Ai%	Ac%
sc 550 nm[1]				*								
abs 550 nm[2]								*	*	*	*	
bsc% 550 nm[3]		*		*								
SSA 550 nm[4]												*
α_{sc} 450/700[5]						*						
α_{bsc} 450/700[6]				*							*	*
T (°C)										*		
pressure								*				
wind speed	*		*									
relative humidity		*		*		*		*		*		*
global radiation										*		
PBL[7]					*							
PM_{10}												
total concentration			*									

[a] Dark and light gray indicate positive and negative (inverse) ($p > 0.95$), while "*"denote weaker ($p > 0.90$) relationships, resp.
(T: total, N: nucleation mode, Ai: Aitken mode, Ac: accumulation mode; [1] scattering at 550 nm; [2] absorption at 550 nm; [3] back scattering at 550 nm; [4] single-scattering albedo at 550 nm; [5] scattering Ångström exponent; [6] backscattering coefficient ; [7] planetary boundary layer).

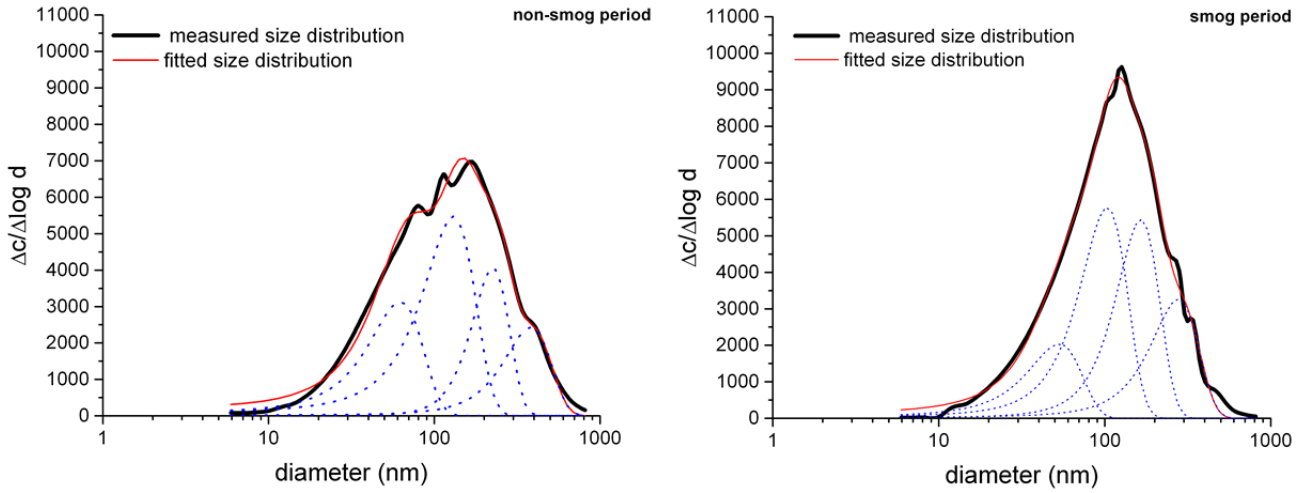

Fig. 3. Measured and fitted aerosol number size distribution during winter smog (a) and non-smog (b) periods. (Under smog and non-smog periods the goodness of the fits were $r^2 = 0.997$ and $r^2 = 0.993$, respectively).

the importance of freshly emitted particles. Contrary, at K-puszta the peak centered at 62 nm indicated that fresh particle formation was not significant; and the modes in the accumulation size range also refer to aged aerosol.

Optical Properties

According to Mészáros *et al.* (1998), at K-puszta, the wintertime average scattering coefficient is 93 Mm^{-1} (λ = 550 nm), which is comparable to the average of non-smog periods (111 Mm^{-1}; Table 4). During smog, the highest total scattering coefficients nearly reached 1000 Mm^{-1}, 800 Mm^{-1} and 500 Mm^{-1} at the wavelengths of 450 nm, 550 nm (see Fig. 2(b)) and 700 nm, respectively. Such high scattering coefficients are generally connected to direct air pollution; e.g., in Guangzhou, Southeast China during a smoky period, the average scattering coefficients were 791 Mm^{-1}, 597 Mm^{-1} and 401 Mm^{-1} at 450 nm, 550 nm and 700 nm, respectively (Garland *et al.*, 2008). At 550 nm, 311 Mm^{-1} was measured under an urban anthropogenic pollution episode in Xin'An (Pan *et al.*, 2009). Extreme scattering coefficients (above 2000 Mm^{-1} at 550 nm) were recorded during the forest fire plumes in August 2005 in Évora, Portugal (Pereira *et al.*, 2011).

The absorption coefficients also increased during the smog episode (see Table 5), however, these values (16.1 and 11.0 Mm^{-1} in the smog episode and beyond this period,

respectively) were significantly lower than the values observed in large cities. In urban air (Reno, Nevada) under winter smog conditions, the scattering and absorption coefficients were nearly twice as high as those on clean days. Estimated from Fig. 6 in Gyawali *et al.* (2012) in Reno the scattering coefficients (at 355, 405, 532, 870nm) were 80, 45, 35, 20 Mm^{-1} (clean days) and 135, 90, 60, 30 Mm^{-1} (polluted days), respectively; while the corresponding values for absorption coefficients were 12.5, 10, 7.5, 5 Mm^{-1} (clean days) and 30, 25, 17, 12 Mm^{-1} (polluted days). Our results showed a similar enhancement of the scattering coefficient, while the increase in the absorption coefficients during the smog was much smaller (32%). Gyawali *et al.* (2012) concluded that the doubling of the absorption coefficient was due to direct traffic emissions. At K-puszta, the lower enhancement of the light absorption may imply that the sampling site is not directly affected by traffic or other emission sources.

Because scattering and absorption coefficients are direct functions of the aerosol (number and mass) concentration, both coefficients had statistically strong linear relationships with PM_{10}, total (TC) and accumulation mode (AcC) number concentrations (Table 5). Using linear regression, 3.5 $m^2\ g^{-1}$ and 0.27 $m^2\ g^{-1}$ average mass scattering and absorption efficiencies (at λ = 550 Mm^{-1}), respectively, were obtained. This mass scattering efficiency is somewhat higher than the values given by, Garland *et al.* (2008) (2.8 $m^2\ g^{-1}$ for Guangzhou, Southeast China, referring to summer of 2006) and Virkkula *et al.* (2011) (2.6 m g^{-1} in Hyytiälä, Finland); however, it is within the range given by Malm and Hand (2007) at IMPROVE sites. In urban environments higher mass scattering and absorption coefficients could be obtained, e.g., fall of 2006 in urban Guangzhou Andreae *et al.* (2008) obtained average values of 4.27 and 0.79 m^2g^{-1}, respectively. At 450 nm and 700 nm, the average scattering efficiencies were 4.8 and 2.2 $m^2\,g^{-1}$, respectively, which are also higher than those obtained for Hyytiälä, Finland (3.7 $m^2\,g^{-1}$ and 1.7 $m^2\,g^{-1}$, respectively) (Virkkula *et al.*, 2011). In addition, the total scattering and absorption coefficients are direct functions of modal diameters (TD, AiD and AcD) and clearly indicate the well-known relationship between optical properties and particle sizes.

The average hemispheric backscatter fraction increased with wavelength (0.10, 0.11 and 0.15 at 450 nm, 550 nm and 700 nm, respectively) and decreased with increasing PM_{10}. b_λ inversely depends on the total mean and accumulation modal diameter: a smaller mean diameter corresponds to a higher effectiveness of backscattering and the aerosol size dependency of the scattering phase function (e.g., Seinfeld and Pandis, 1998). During the smog episode, b_λ decreased by 8% (450 nm), 9% (550 nm) and 10% (700nm) compared to the non-smog period.

The single scattering albedo (SSA) in January–February 2010 (0.91) was similar to the values obtained for other sites e.g., Virkkula *et al.* (2011). Under the smog episode, the average SSA increased by 2% which is related to the increase in the PM_{10} and the greater increase in the scattering relative to the absorption coefficient. This high SSA generally indicates well-aged regional haze aerosol which is characterized by more scattering and less absorbing properties (e.g., Andreae *et al.*, 2008). A haze event in Leipzig, Germany was attributed to regional transport and consisted of a mixture of urban and Arctic haze aerosols (Müller *et al.*, 2004); the single-scattering albedo was similarly as high (0.97 ± 0.06 at 532 nm) as that observed at K-puszta.

The average Ångström exponent (α) of the total scattering coefficients was above 1.9 for the wavelength pair of 450/700 nm (Table 4). The high values also show that at K-puszta, the aerosol is aged and is generally dominated by fine fraction (Wang *et al.*, 2015). This is further supported by the Ångström exponents of well-aged aerosol (1.8–2.8; wavelength range: 355–532 nm) presented by Müller *et al.* (2004). During the smog episode, the exponent decreased (see also Wu *et al.*, 2015) as a result of the increase in the modal diameter, which is consistent with the inverse relationship between the Ångström exponent and aerosol size. For backscattering, the wintertime average Ångström exponent was 1.01 (450/700 nm).

The Effect of Meteorological Parameters on Aerosol Properties

The statistical relationship of aerosol properties to meteorological parameters is summarized in Table 5. We found that meteorological parameters mostly influence PM_{10} and the number concentration in the accumulation mode (AcC); as a consequence, the aerosol optical properties (scattering and absorption coefficients) are affected. As mentioned, the development of a high-pressure system had an important effect on the PM_{10} concentration. Along with rising surface pressure and decreasing temperature and wind speed, a high level of PM_{10} was measured. Because PM_{10} is mainly governed by the number concentration in the accumulation mode, AcC varies similarly to PM_{10}, along with the variation of these meteorological parameters. As the high-pressure system developed, the AcC increased by ~50%.

Variation in the surface pressure, temperature and wind speed was also reflected in the total mean diameter (TD). In addition, higher RH results in larger TD and AiD. The daily variation in the RH and AiD indicate that Aitken mode particles could be hygroscopic. However, the accumulation modal diameter (AcD) is not affected by relative humidity. Generally, particle growth is linked to vapor – including water vapor – that condenses on the particles. Aitken mode particles are significantly smaller than particles in the accumulation mode; because of water vapor condensation, the change in the AiD size is much more distinct than in the accumulation mode. Finally, the nucleation mode diameter (ND) was not noticeably affected by the meteorological parameters, including the global radiation.

Among the modal fractions, N% was positively correlated with global radiation, wind speed and temperature but negatively correlated with RH. Ai% and Ac% varied oppositely as functions of air pressure, temperature and wind, as shown in Table 5. All these variations reflect the development of the high-pressure system.

Because of the changes in the meteorological parameters,

the scattering and absorption coefficients varied similarly to the PM_{10} and number concentrations. In addition, as the height of the planetary boundary layer lowered, the scattering coefficient increased. The high-pressure buildup decreased the backscatter fraction and the Ångström exponent, most likely due to the growth of the average particle size. Finally, under the high-pressure system, the SSA increased as a result of the greater increase in the scattering coefficient than in the absorption coefficient.

The effect of regional air pollution on the background air quality at K-puszta can be collated by comparing parallel PM_{10} concentrations and aerosol extinction coefficients measured in Budapest and K-puszta (Fig. 2). The extinction coefficients in Budapest were derived from visual range observations (e.g., Molnár *et al.*, 2008). The average PM_{10} concentration at K-puszta was generally the same as that in Budapest (49.9 and 44.9 μgm^{-3}, respectively). During the smog, the average PM_{10} in Budapest increased by 40% compared to non-smog period, while at K-puszta the average concentration nearly doubled. This parallel variation of wintertime PM_{10} concentration in Budapest and at K-puszta is rather common as shown in Table 1 for the periods from December to February between 2007 and 2012. The direct relationship between the enhanced PM_{10} concentration and permanent inversion periods resulting occasionally in heavy smog periods is affirmed.

At K-puszta, the average dry extinction (scattering + absorption) coefficient at 550 nm was 189 Mm^{-1}, while a similar value (255 Mm^{-1}) was obtained in Budapest. Under smog a 1.5 times increase in the dry extinction coefficient was observed in Budapest while at K-puszta the corresponding value was 1.9. These data directly imply that air pollution in Hungary (Central Europe) is not confined to the large cities; it actually causes serious problems outside of towns and in rural areas. This is further supported by the spatial distribution of PM_{10} during January–February, 2010. In Fig. 4 PM_{10} concentrations during the smog and non-smog periods are shown for different parts of Hungary representing mainly urban environment (Hungarian Air Quality Network) and at K-puszta). It has to note that at all sampling sites the PM_{10} concentration was significantly (average: 180%, range: 150%–225%) higher during the smog than non-smog period. Despite the greatly different environments during the smog the average PM_{10} concentrations were rather comparable at all sites. This similarity directly indicates the importance of regional transport in PM_{10} concentration.

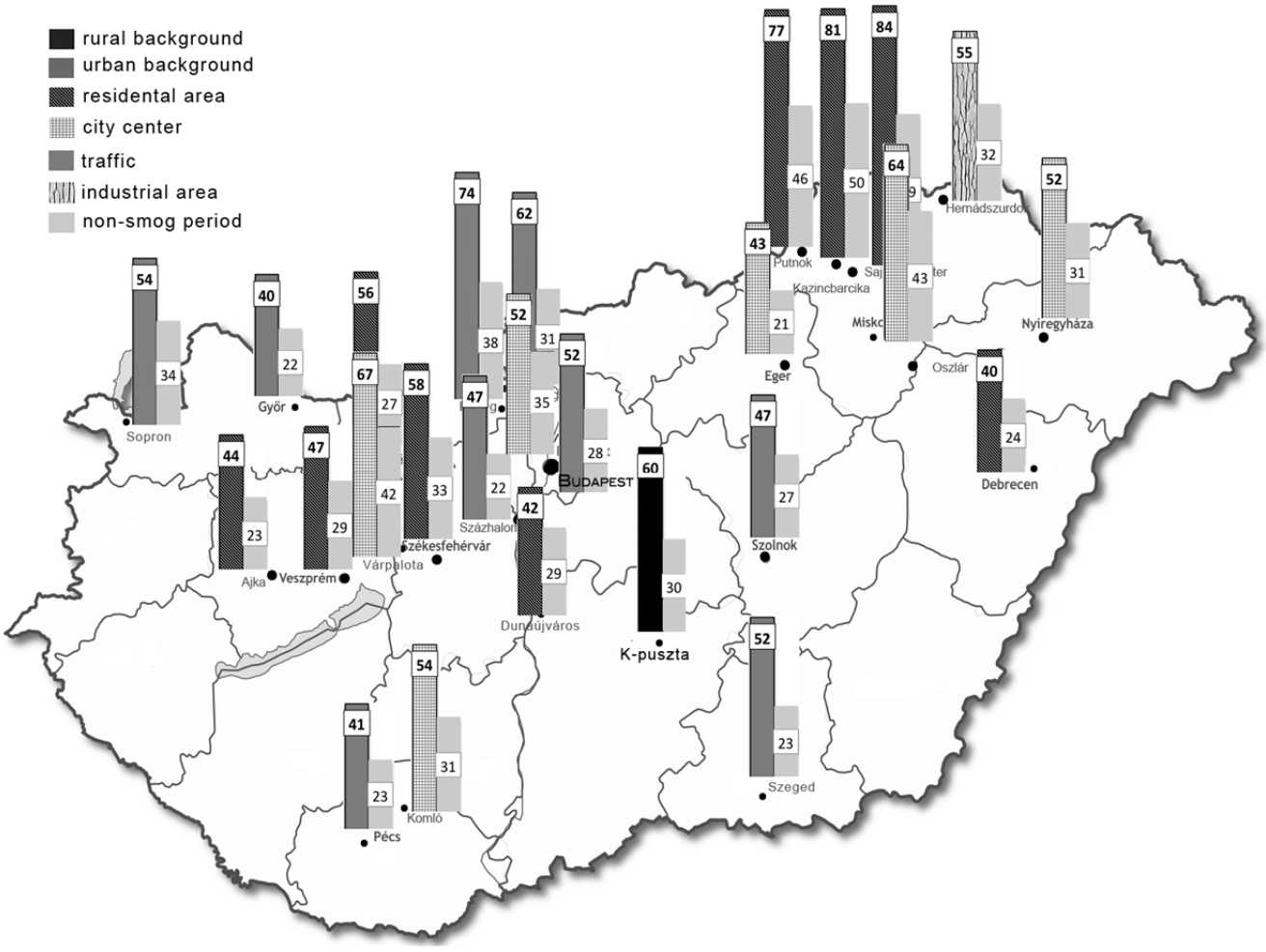

Fig. 4. Spatial variation of average (2 months) PM_{10} concentration in Hungary, January–February, 2010. Data are from Hungarian Air Quality Network and Hungarian Meteorological Service (K-puszta).

CONCLUSIONS

In this work, we summarized the physical properties of wintertime aerosol and the effects of a high-pressure blocking condition on regional, rural aerosols based on observations conducted at the K-puszta station in Hungary. K-puszta is a rural site that is not directly influenced by local emissions; it is as far from direct anthropogenic pollution sources as possible. Our results indicate that the air quality at K-puszta is often influenced by regional air pollution, particularly in winter. High-pressure blocking events have significant impacts on the physical properties of rural aerosols and on particle formation processes. The most significant impacts of extreme episodes are manifested as changes in the PM_{10} concentrations and, in the aerosol optical properties. The scattering and absorption coefficients increased considerably and reached extreme values that are characteristic of a heavily polluted atmosphere rather than rural air. Considering the lack of important local sources, these changes in PM_{10} could be attributed to regional-scale transport. We can conclude that the aerosol properties at K-puszta are characterized by a large spatial extent. Further, an important aspect should also be considered when air pollution is studied and evaluated: beside the emissions of certain pollutants the trends in air pollution very much depend on the meteorological conditions in the Carpathian basin. Based on our results, it can be concluded that the aerosol measured at K-puszta is generally dominated by fine fraction which is supported by recently started $PM_{2.5}$ measurements. This is clearly indicated by the correlation coefficients between PM_{10} and the number concentration or the modal fraction of the accumulation mode, as well as the high values of the Ångström exponents.

ACKNOWLEDGEMENTS

The research leading to these results has received funding from the European Union Seventh Framework Programme (FP7/2007-2013) under grant agreement n° [262254], [ACTRIS]; and TÁMOP-4.2.2.A-11/1/KONV-2012-0064: Regional effects of weather extremes resulting from climate change and potential mitigation measures in the coming decades (The project is realized with the support of the European Union, with the co-funding of the European Social Fund). The authors greatly acknowledge the Department of Physics, University of Helsinki for providing the DMPS measurements and size distribution data.

REFERENCES

Aalto, P., Hämeri, K., Becker, E., Weber, R., Salm, J., Mäkelä, J.M., Hoell, C., O'Dowd, C.D., Karlsson, H., Hansson, H.C., Väkevä, M., Koponen, I.K., Buzorius, G. and Kulmala, M. (2001). Physical characterization of aerosol particles during nucleation events. *Tellus Ser B* 53: 344–358.

Anderson, T.L. and Ogren, J.A. (1998). Determining aerosol radiative properties using the TSI3563 integrating nephelometer. *Aerosol Sci. Technol.* 29: 57–69, doi: 10.1080/02786829808965551.

Anderson, T.L., Covert, D.S., Marshall, S.F., Laucks, M.L., Charlson, R.J., Waggoner, A.P., Ogren, J.A., Caldow, R., Holm, R.L., Quant, F.R., Sem, G.J., Wiedensohler, A., Ahlquist, N.A. and Bates, T.S. (1996). Performance characteristics of a high-sensitivity, three-wavelength total scatter/backscatter nephelometer. *J. Atmos. Oceanic Technol.* 13: 967–986, doi: 10.1175/1520-0426(1996)013<0967:PCOAHS>2.0.CO;2.

Andreae, M.O., Schmid, O., Yang, H., Chand, D., Yu, J.Z., Zeng, L.M. and Zhang, Y.H. (2008). Optical properties and chemical composition of the atmospheric aerosol in urban Guangzhou, China. *Atmos. Environ.* 42: 6335–6350, doi: 10.1016/j.atmosenv.2008.01.030.

Baranova, A. and Hovorka, J. (2013). Atmospheric Aerosol Size Distribution during Winter Period in Ostrava-Radvanice. EAC 2013, European Aerosol Conference Prague, Czech Republic, 1–6 September 2013.

Bécsi, Zs., Molnár, A., Imre, K. and Aalto, P.P. (2013). Characteristics of New Particle Formation Events in Hungarian Background air at K-puszta, 2008-2012. EAC 2013, European Aerosol Conference Prague, Czech Republic, 1-6 September 2013.

Bond, T.C., Anderson, T.L. and Campbell, D. (1999). Calibration and intercomparison of filterbased measurements of visible light absorption by aerosols. *Aerosol Sci. Technol.* 30: 582–600, doi: 10.1080/02786829930443 5.

Breiling, M., (1993). *Emergency Air Protection: Implementing Smog Alarm Systems in Central and Eastern Europe*. International Institute for Applied Systems Analysis, Laxenburg, Austria.

Cséki, G. (2010). *Formation of Inversions in the Carpathian-Basin*. Diploma work, Eötvös Loránd University, Budapest. (In Hungarian)

Dal Maso, M., Kulmala, M., Riipinen, I., Wagner, R., Hussein, T., Aalto, P.P. and Lehtinen, K.E.J. (2005). Formation and growth of fresh atmospheric aerosols: eight years of aerosol size distribution data from SMEAR II, Hyytiälä, Finland. *Boreal Environ. Res.* 10: 323–336.

EEA (2013). Air Quality in Europe — 2013 Report. European Environmental Agency Report, EEA Report No 9/2013, Luxenbourg.

Ferenczi, Z. (2013). Predictability analysis of the $PM_{2.5}$ and PM_{10} concentration in Budapest. *Időjárás* 117: 359–375.

Garland, R.M., Yang, H., Schmid, O., Rose, D., Nowak, A., Achtert, P., Wiedensohler, A., Takegawa, N., Kita, K., Miyazaki, Y., Kondo, Y., Hu, M., Shao, M., Zeng, L.M., Zhang, Y.H., Andreae, M.O. and Pöschl, U. (2008). Aerosol optical properties in a rural environment near the mega-city Guangzhou, China: implications for regional air pollution, radiative forcing and remote sensing. *Atmos. Chem. Phys.* 8: 5161–5186.

Guo, S., Hu, M., Zamora, M. L., Peng, J., Shang, D., Zheng, J., Du, Z., Wua, Z., Shao, M., Zeng, L., Molina, M. J. and Zhang, R. (2014). Elucidating severe urban haze formation in China. *Proc. Natl. Acad. Sci. U.S.A.* 111: 17373–17378, doi: 10.1073/pnas.1419604111.

Gyawali, M., Arnott, W.P., Zaveri, R.A., Song, C., Moosmüller, H., Liu, L., Mishchenko, M.I., Chen, L.W.A., Green, M.C., Watson, J.G. and Chow, J.C. (2012). Photoacoustic optical properties at UV, VIS, and near IR wavelengths for laboratory generated and winter time ambient urban aerosols. *Atmos. Chem. Phys.* 12: 2587–2601, doi: 10.5194/acp-12-2587-2012.

Hungarian Air Quality Network, http://www.levegominoseg.hu/automata-merohalozat.

Jiang, J., Zhou, W., Cheng, Z., Wang, S., He, K. and Hao, J. (2015). Particulate matter distributions in China during a winter period with frequent pollution episodes (January 2013). *Aerosol Air Qual. Res.* 15: 494–503, doi: 10.4209/aaqr.2014.04.0070.

Junge, C.E. (1963). *Air Chemistry and Radioactivity*. Academic Press, New York, London, p. 142–146.

Larsen, B.R., Junninen, H., Mønster, J., Viana, M., Tsakovski, P., Duvall, R.M., Norris, G.X. and Querol, X. (2008). The Krakow Receptor Modelling Inter-comparison Exercise. European Commission, Joint Research Centre, Institute for Environment and Sustainability, Luxembourg.

Malm, W.C. and Hand, J.L. (2007). An examination of the physical and optical properties of aerosols collected in the IMPROVE program. *Atmos. Environ.* 41: 3407–3427.

Mészáros, E., Molnár, A. and Ogren, J.A. (1998). Scattering and absorption coefficients vs. chemical composition of fine atmospheric aerosol particles under regional conditions in Hungary. *J. Aerosol Sci.* 29: 1171–1178.

Molnár, A., Mészáros, E., Imre, K. and Rüll, A. (2008). Trends in visibility over Hungary between 1996 and 2002. *Atmos. Environ.* 42: 2621–2629, doi: 10.1016/j.atmosenv.2007.05.012

Müller, D., Mattis, I., Ansmann, A., Wehner, B., Althausen, D., Wandinger, U. and Dubovik, O. (2004). Closure study on optical and microphysical properties of a mixed urban and Arctic haze air mass observed with Raman lidar and Sun photometer. *J. Geophys. Res.* 109: D13206, doi: 10.1029/2003JD004200.

Müller, T., Henzing, J.S., de Leeuw, G., Wiedensohler, A., Alastuey, A., Angelov, H., Bizjak, M., Collaud Coen, M., Engström, J.E., Gruening, C., Hillamo, R., Hoffer, A., Imre, K., Ivanow, P., Jennings, G., Sun, J.Y., Kalivitis, N., Karlsson, H., Komppula, M., Laj, P., Li, S.M., Lunder, C., Marinoni, A., Martins dos Santos, S., Moerman, M., Nowak, A., Ogren, J.A., Petzold, A., Pichon, J.M., Rodriquez, S., Sharma, S., Sheridan, P.J., Teinilä, K., Tuch, T., Viana, M., Virkkula, A., Weingartner, E., Wilhelm, R. and Wang, Y.Q. (2011). Characterization and intercomparison of aerosol absorption photometers: result of two intercomparison workshops. *Atmos. Meas. Tech.* 4: 245–268, doi: 10.5194/amt-4-245-2011.

Pan, X.L., Yan, P., Tang, J., Ma, J.Z., Wang, Z.F., Gbaguidi, A. and Sun, Y.L. (2009). Observational study of influence of aerosol hygroscopic growth on scattering coefficient over rural area near Beijing mega-city. *Atmos. Chem. Phys.* 9: 7519–7530, doi: 10.5194/acp-9-7519-2009.

Pereira, S.N., Wagner, F. and Silva, A.M. (2011). Seven years of measurements of aerosol scattering properties, near the surface, in the southwestern Iberia Peninsula. *Atmos. Chem. Phys.* 11: 17–29, doi: 10.5194/acp-11-17-2011.

Quinn, P.K., Shaw, G., Andrews, E., Dutton, E.G., Ruoho-Airola, T. and Gong, S.L. (2007). Arctic haze: current trends and knowledge gaps. *Tellus Ser* B 59: 99–114.

Ram, K., Sarin, M.M., Sudheer, A.K. and Rengarajan, R. (2012). Carbonaceous and Secondary inorganic aerosols during wintertime fog and haze over urban sites in the Indo-Gangetic Plain. *Aerosol Air Qual. Res.* 12: 359–370, doi: 10.4209/aaqr.2011.07.0105.

Richter, D. and Peter Williams, W. (1998). Assessment and Management of Urban Air Quality in Europe. Monitoring and Assessment Research Centre (MARC), King's College London, EEA Monograph No.5.

Seinfeld, J.H. and Pandis, S.N. (1998). *Atmospheric Chemistry and Physics. From Air Pollution to Climate Change.* John Wiley and Sons, Inc., New York, Chichester, Weinheim, Brisbane, Singapore, Toronto.

UWYO, University of Wyoming, College of Engineering, Department of Atmospheric Science Atmospheric Soundings, http://weather.uwyo.edu/upperair/sounding.html.

Virkkula, A., Backman, J., Aalto, P.P., Hulkkonen, M., Riuttanen, L., Nieminen, T., Dal Maso, M., Sogacheva, L., de Leeuw, G. and Kulmala, M. (2011). Seasonal cycle, size dependencies, and source analyses of aerosol optical properties at the SMEAR II measurement station in Hyytiälä, Finland. *Atmos. Chem. Phys.* 11: 4445–4468, doi: 10.5194/acp-11-4445-2011.

Wang, L., Gong, W., Singh R., Xiangao, X., Huizheng, C., Zhang, M. and Hong, L. (2015). Aerosol optical properties over Mount Song, a rural site in central China. *Aerosol Air Qual. Res.* 15: 2051–2064, doi: 10.4209/aaqr.2014.12.0335.

Wu, Y., Yan, P., Tian, P., Tao, J., Li, L., Chen, J., Zhang, Y., Cao, N., Chen, C. and Zhang, R. (2015). Spectral light absorption of ambient aerosols in urban Beijing during summer: An intercomparison of measurements from a range of instruments. *Aerosol Air Qual. Res.* 15: 1178–1187, doi: 10.4209/aaqr.2014.09.0224

Yli-Juuti, T., Riipinen, I., Aalto, P.P., Nieminen, T., Maenhaut, W., Janssens, I.A., Claeys, M., Salma, I., Ocskay, R., Hoffer, A., Imre, K. and Kulmala, M. (2009). Characteristics of new particle formation events and cluster ions at K-puszta, Hungary. *Boreal Environ. Res.* 14: 683–698.

Yuan, Q., Li, W., Zhou, S., Yang, L., Chi, J., Sui, X. and Wang, W. (2015). Integrated evaluation of aerosols during haze-fog episodes at one regional background site in North China Plain. *Atmos. Res.* 156: 102–110, doi: 10.1016/j.atmosres.2015.01.002.

Zheng, G.J., Duan, F.K., Su, H., Ma, Y.L., Cheng, Y., Zheng, B., Zhang, Q., Huang, T., Kimoto, T., Chang, D., Pöschl, U., Cheng, Y.F. and He, K.B. (2015). Exploring the severe winter haze in Beijing: The impact of synoptic weather, regional transport and heterogeneous reactions. *Atmos. Chem. Phys.* 15: 2969–2983, doi: 10.5194/acp-15-2969-2015

Zotter, P., Ciobanu, V.G., Zhang, Y.L., El-Haddad, I., Macchia, M., Daellenbach, K.R., Salazar, G.A., Huang, R.J., Wacker, L., Hueglin, C., Piazzalunga, A., Fermo, P., Schwikowski, M., Baltensperger, U., Szidat, S. and Prévôt, A.S.H. (2014). Radiocarbon analysis of elemental and organic carbon in Switzerland during winter-smog episodes from 2008 to 2012 – Part 1: Source apportionment and spatial variability. *Atmos. Chem. Phys.* 14: 13551–13570, doi: 10.5194/acp-14-13551-2014.

Received for review, April 1, 2015
Revised, February 26, 2016
Accepted, June 23, 2016